A Letters Journal Exploring the Frontiers of Physics

October 2009

EPL, **88** (2009) 20006
doi: 10.1209/0295-5075/88/20006

www.epljournal.org

Experimental observation of trapped modes in a water wave channel

P. J. Cobelli[1(a)], V. Pagneux[2], A. Maurel[3] and P. Petitjeans[1]

[1] *Laboratoire de Physique et Mécanique des Milieux Hétérogènes, UMR CNRS 7636, Ecole Supérieure de Physique et de Chimie Industrielles - Paris, France, EU*
[2] *Laboratoire d'Acoustique de l'Université du Maine, UMR CNRS 6613, Université du Maine - Le Mans, France, EU*
[3] *Laboratoire Ondes et Acoustique, Institut Langevin, UMR CNRS 7587, Ecole Supérieure de Physique et de Chimie Industrielles - Paris, France, EU*

received 24 July 2009; accepted in final form 1 October 2009
published online 4 November 2009

PACS 03.65.Ge – Solutions of wave equations: bound states
PACS 43.20.Ks – Standing waves, resonance, normal modes
PACS 47.35.Lf – Wave-structure interactions

Abstract – The fluid around a free surface piercing circular cylinder in a long narrow wave tank can exhibit a local oscillation that does not propagate down the channel but is confined to the vicinity of the cylinder. This is a manifestation of the so-called trapped modes, bound states in the continuum occurring in many situations in physics. In this letter, using Fourier Transform Profilometry, fully space time resolved measurements for the free surface deformation are obtained. The scattering characteristics of the cylinder and consequently the behavior of the trapped-mode frequency are determined.

Trapped modes have been studied in many domains of physics (for a review, see [1]), elastic waves [2,3], water waves [4–8] or electromagnetic waves [9,10]. They are finite-energy solutions to the wave equation in infinite domain with discrete eigenvalues embedded in the continuous spectrum. Trapped modes have to be distinguished from scattering states whose eigenvalues are in the continuous spectrum and that have infinite energy. Experimentally, trapped modes turn into quasi-trapped modes that can be evidenced by scattering resonances. This is due to deviations in the experiments with respect to the theoretical configuration: finite-size effect producing radiation toward infinity or leaking due to dissipative mechanisms. However, the study of quality factors of the trapped-mode resonances is of interest. Indeed, high-quality factors in trapped-mode resonances are decisive for the design of metamaterials, whose remarkable properties, such as negative index or cloaking, are underpinned by the resonant nature of their response.

Among the physical situations giving rise to trapped-mode resonances, the case of water waves is of particular interest. Firstly, water wave resonances have many practical applications in naval and coastal engineering [11,12]. In addition to their own interest, water waves exhibit similar properties as electromagnetic and microwaves, *e.g.* negative refraction or cloaking [13–15]. From that point of view, water waves are attractive since the wave field is the free surface deformation, that is already qualitatively accessible to the naked eye.

In this letter, we study experimentally the trapped-mode resonances of water waves interacting with a cylindrical obstacle in a waveguide. This configuration has been studied in linearized water wave theory by [4–7] and very few experimental results are available [16]. Also, it corresponds to the problem of an infinite set of cylinders where strong resonances have been numerically observed [12].

Owing to Fourier Transform Profilometry [17–19], we get a resolution of the surface elevation in time and in space able to quantitatively describe the trapped-mode resonances, by means of their patterns and by means of the reflection and transmission coefficients. A model for the frequency dependence of the scattering data, influenced by the proximity of the threshold for propagation, is proposed and compared favorably with the experimental results.

Our experimental set-up consists of a water tank with constant water level at rest which is chosen to be fixed at $h_0 = 5\,\mathrm{cm}$. The system of interest is placed inside the tank: a waveguide formed by two parallel vertical walls,

(a) E-mail: cobelli@pmmh.espci.fr

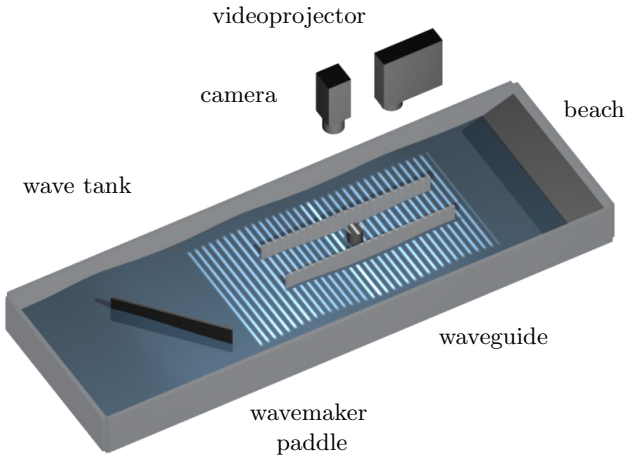

(a) Scheme of the complete experimental set-up.

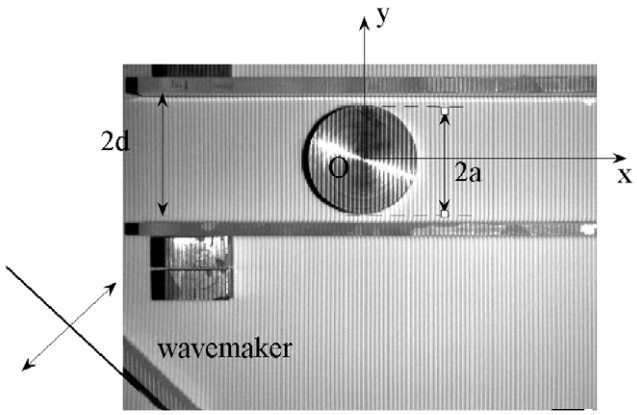

(b) Camera's view.

Fig. 1: (Color online) Experimental set-up (a). Symmetric and antisymmetric modes are generated at the entrance of the waveguide by the wavemaker. A free surface piercing circular cylinder of diameter $2a \in [2, 10]$ cm lies in the center of the waveguide of width $2d = 10$ cm. The measurement is performed using an optical method (Fourier Transform Profilometry). A videoprojector projects fringes onto the free surface and the image is collected by a camera. Analysis of the fringe displacements allows for the reconstruction of the surface deformation at each pixel. Panel (b) presents a sample of the camera's view showing the free surface and the projected fringes, the waveguide, the cylinder, and a portion of the wavemaker paddle.

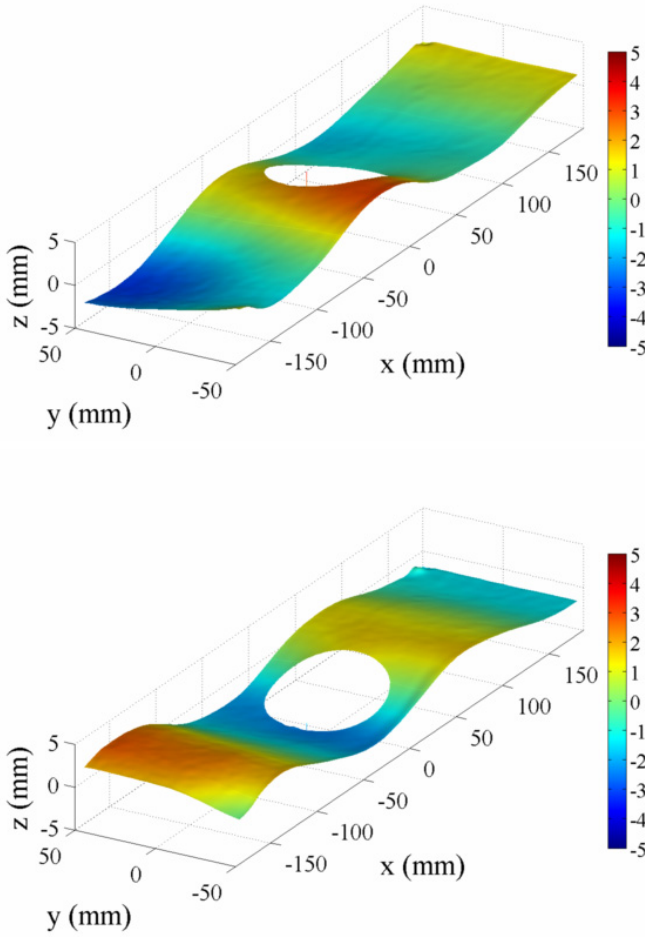

Fig. 2: (Color online) Typical instantaneous fields of the surface elevation $h_T(x, y, t)$, here for $a/d = 0.50$, $kd = 1.32$. The scale of the colorbar is in mm.

60 cm long, a distance $2d = 10$ cm apart, has a free surface piercing vertical circular cylinder of diameter $2a$ ($a = 1$ to 5 cm) located symmetrically between the two walls (fig. 1). Water waves are generated by a wave maker forming an angle of around 45° with the waveguide axis Ox (so symmetric and antisymmetric modes are generated at the entrance of the waveguide) at a frequency $f \in [2, 3]$ Hz.

An important specificity in our experiment is the measurement of the surface elevation. This optical method, termed Fourier Transform Profilometry, is originally due to [17] and has been described in [18,19] for application to water wave measurements. By projecting fringes onto the free surface and by analyzing the fringe displacement, we are able to deduce the surface elevation in the working window. In the present experiment, the window is $40 \times 10\,\text{cm}^2$ corresponding to $1623 \times 421\,\text{pixels}^2$. The width of the pixel, 0.23 mm, sets the spatial resolution and the resolution on the surface elevation. The temporal resolution is only limited by the acquisition rate of the camera since a single picture is needed to get the measurement. In our experiment, a high speed camera is used with an acquisition rate close to 300 Hz.

Typical free surface deformation fields $h_T(x, y, t)$ near resonance are shown in fig. 2. The acquisition rate of the camera is synchronized with the wavemaker in order to get 200 acquisitions $h_T(x, y, t)$ over two periods of the water wave oscillation. For a perfect fluid, in absence of dissipation, the dispersion relation for the water waves is given by $\omega^2 = gk \tanh kh_0$ where ω is the driving pulsation, k the wave number and $g = 9.81\,\text{m} \cdot \text{s}^{-2}$. For the purposes of this study, the effects of surface tension will be neglected.

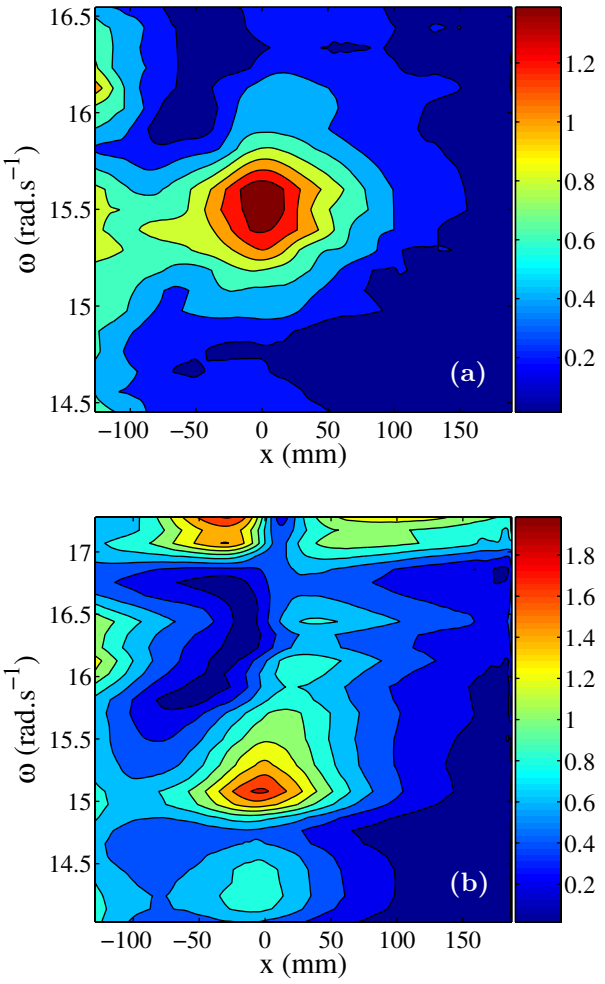

Fig. 3: (Color online) Evidence of the trapped-mode resonances: $(h_T(x,y,t)-h_T(x,-y,t))/2$ for some fixed y is displayed in colorscale as a function of x and ω. (a) for $a/d=0.50$, one resonance is visible near the cylinder and (b) for $a/d=0.85$, in addition to the first resonance, a second maximum near the cutoff frequency can be seen (the cylinder lies at $x=0$). The scale of the colorbar is in mm.

A first direct qualitative evidence of the resonance phenomenon can already be obtained from these instantaneous fields. The symmetry of the geometry decouples the fields into two families, even and odd with respect to y. The wave is always propagative for the first family while it has a non zero cut on frequency for the second family. This latter gap property enables the existence of the trapped mode [20]. Figure 3 shows the odd family, $[h_T(x,y,t)-h_T(x,-y,t)]/2$, for some given y and t as a function of x and ω. Typical spots are visible that are indicative of the presence of resonances.

In order to obtain quantitative characterics of the resonance, we extract, at each position, the coefficient $h_1(x,y)$ of the Fourier series

$$h_T(x,y,t)=\sum_n h_n(x,y)e^{in\omega t}. \qquad (1)$$

This is achieved owing to the large sampling rate offered by the camera. In our experiment, the weight of the non linearities $|h_T-h_1|/|h_T|$ is less than 15%. h_1 is then separated into an even part h^e and an odd part h^o. Figure 4 depicts the typical situation near resonance: the trapped mode is isolated in the odd part of the field and is localized in the vicinity of the cylinder. Depending on the geometry, it is either symmetric with respect to the vertical axis, as predicted in ref. [20] or antisymmetric with respect to the vertical axis as predicted in ref. [21]. This latter trapped mode is expected to exist only for $a/d \gtrsim 0.81$ [21], what we experimentally confirm. The even field h^e makes the propagative plane mode to appear. This field is used to get a direct measurement of the wave number k. The agreement with the theoretical dispersion relation is of about 2%.

To go further, we want to get a 1D model. With a constant water level at rest h_0, the free surface elevation $h_1(x,y)$ is governed by the Helmholtz equation $(\Delta+k^2)h_1(x,y)=0$, with Neumann boundary condition at the walls, where k is given by the aforementioned dispersion relation [22]. Then, in our analysis, the odd part $h^o(x,y)$ of the field $h_1(x,y)$ is modelized in a 1D problem by projecting the 2D field onto the first transverse mode:

$$h^o(x,y)\simeq h(x)\sin \pi y/2d, \qquad (2)$$

outside of the near field of the cylinder (fig. 5(a)). In the near field, the higher transverse modes are expected to contribute to the 2D solution. However, the contribution of the higher-order modes (with $\sin(2n+1)\pi y/2d$, $n\neq 0$ dependence) is less than 7% in our experiments. The typical behavior of $h(x)$ is shown in fig. 5(b). Because we are working below the first cutoff frequency, at $\pi/(2d)$, for antisymmetric modes, the solution is sought as

$$\begin{aligned} h(x<0) &= A\,e^{-\alpha x}+AR\,e^{\alpha x},\\ h(x>0) &= AT\,e^{-\alpha x}, \end{aligned} \qquad (3)$$

with A the amplitude of the incident wave, α the wave number of the first evanescent mode and (R,T) the reflection and transmission coefficients. Such behavior is illustrated in fig. 5.

The reflection and transmission coefficients (R,T) and α are fitted for each frequency outside the near-field region. The resonance curves are obtained, as exemplified in fig. 6 for $a/d=0.50$ (the single resonance corresponds to a trapped mode as in fig. 4(b)) and for $a/d=0.85$ (the two resonances correspond to the two types of trapped modes in fig. 4(b), (d)).

As is evident from these curves, the classical Breit-Wigner resonance shape is not well suited as it would be unable to reproduce their clear asymmetry. We have checked that this asymmetry is not an experimental artifact by computing the transmission and reflection coefficients numerically (numerical calculations have been performed using the toolbox PDEtool of Matlab; see

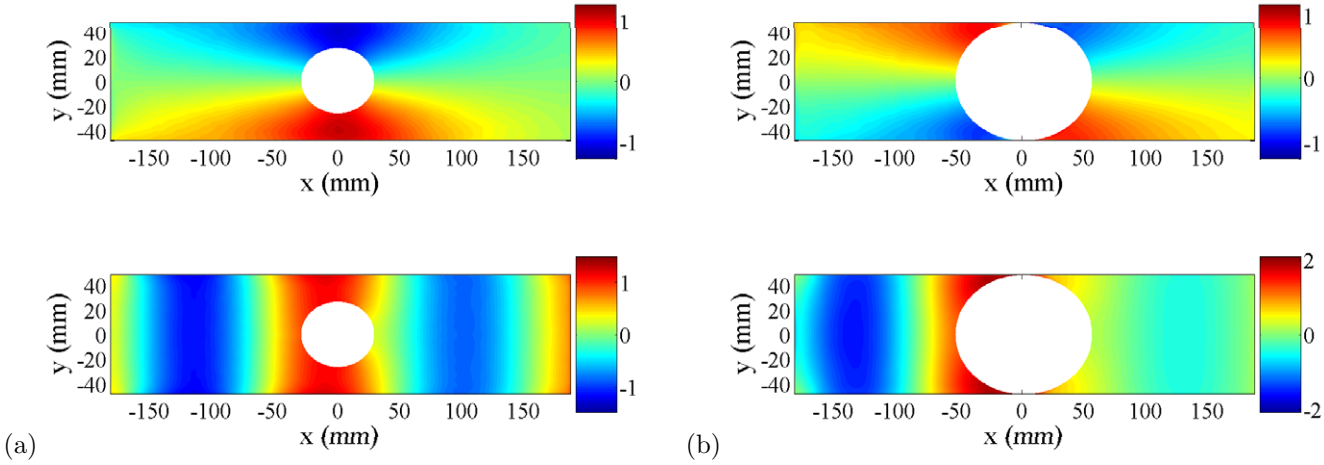

Fig. 4: (Color online) Experimental patterns of the two trapped modes, and the associated even parts. (a) Even and odd fields of the linear field $h_1(x,y)$, for $a/d=0.40$ and $kd=1.46$. The even part exhibits the form of the trapped-mode localized in the vicinity of the cylinder. (b) Same representation for $a/d=0.95$ and $kd=1.51$. The scale of the colorbar is in mm.

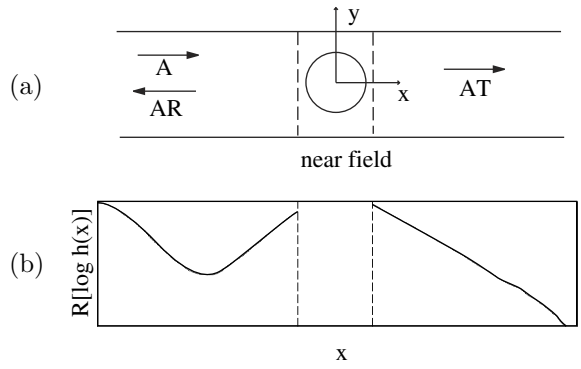

Fig. 5: Top: the problem reduces to a 1D problem along the x-axis, by projecting the odd field onto the first transverse mode in $\sin \pi y/2d$ outside the near-field region. Bottom: typical variation of the measured $h(x)$ along the x-axis: real part of $\log[h(x)]$ as a function of x (a.u.) (the curve has been obtained for $a/d=0.4$, $kd=1.47$).

footnote [1]). The 1D transmission and reflection coefficients are actually influenced by the proximity of the cutoff frequency at $kd=\pi/2$. It has been already observed for confined states in bent waveguides in [23] that proposed the following asymmetric shape for T:

$$T=\frac{B}{1-C/(\alpha d)}, \qquad (4)$$

where $\alpha d \equiv \sqrt{(\pi/2)^2-(kd)^2}$. This equation has to be understood in the neighbourhood of the resonance in the complex plane. The constants B and C have been numerically computed and we have checked that eq. (4) is valid in the complex k-plane. Note that (B,C) are functions of the geometry only. For $a/d=0.50$, we have found $B=1.15$ and $C=0.73$. For $a/d=0.85$, there are two resonances and the transmission coefficient can be written as the sum of two shapes, each of them given by eq. (4); with $B_1=1.85$, $C_1=0.8325$ and $B_2=-1.2$, $C_2=0.135$.

In the experiment, a small attenuation is present that is modelized by a small imaginary part of k. This attenuation can only be roughly evaluated, because of a low signal to noise ratio on the imaginary part of α. The experimental measurements of α gives, through the relation $k=\sqrt{(\pi/2d)^2-\alpha^2}$, an estimation of $\mathrm{Im}(k)d\sim 0.03$.

As shown in fig. 6, a good agreement is observed between the experiments and the prediction of eq. (4). For the case $a/d=0.50$ in fig. 6(a), a constant attenuation $\mathrm{Im}(k)d=0.025$ has been used, a value consistent with our rough experimental estimate. For the case $a/d=0.85$ in fig. 6(b), the second resonance is visible, a fact that can be reproduced only assuming a significant decrease in the attenuation from $\mathrm{Im}(k)d=0.033$ near the first resonance to 0.003 near the second resonance.

The behavior of the resonance frequency $k_c d$ when changing the size of the cylinder is shown in fig. 7. There are two branches: the first corresponds to trapped modes symmetric with respect to Oy-axis and the second to trapped modes antisymmetric with respect to Oy-axis.

The experimental results are compared to the theoretical predictions of ref. [20] for the first branch and with the theoretical predictions of ref. [21] for the second branch. The authors in [21] predicted that the resonances of the second branch exist for $a/d \gtrsim 0.81$. This prediction is confirmed here. An excellent agreement is observed with the theoretical predictions for both branches. It is worth

[1] The numerics has been performed using the toolbox PDEtool of Matlab. The equation is the Helmholtz equation $(\Delta+k^2)\phi=0$, with vanishing normal gradient on the cylinder boundary and the lateral walls. The leading antisymmetric mode (with $\sin \pi y/2d$ transverse dependence) is imposed at the entrance. Then, the transmitted and reflected waves are collected in the far field of the cylinder.

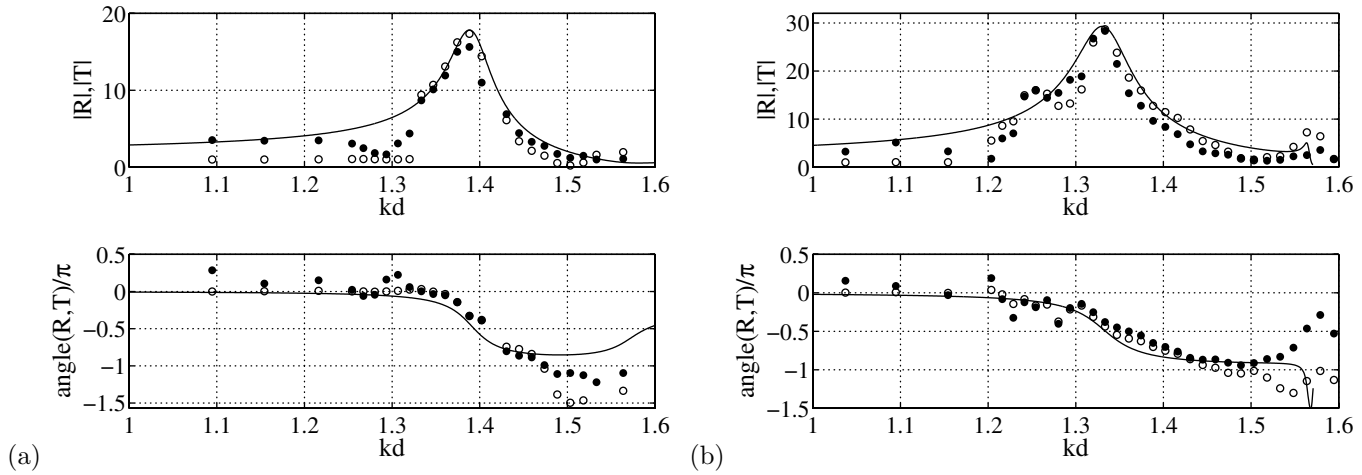

Fig. 6: Resonance curves for (a) $a/d = 0.50$ and (b) $a/d = 0.85$, upper panel $|R|$ (plain circle), $|T|$ (open circle) as a function of the wave number kd. Lower panels show the corresponding phases. Plain lines correspond to the results obtained from numerical calculations, indiscernible from the expression in eq. (4).

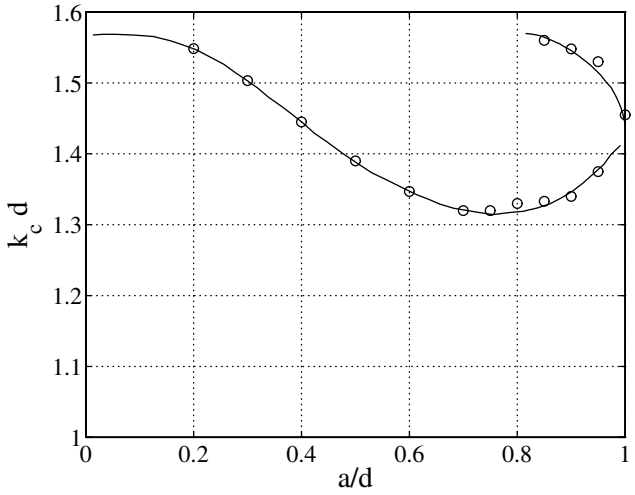

Fig. 7: Resonance frequencies $k_c d$ as a function of a/d. Open circles are the experimental values deduced from the resonance curves and plain lines are the theoretical predictions from [20, 21].

noting that this is the case even for the largest values of a/d, for which the effect of a meniscus in the small region between the cylinder and the waveguide walls would seem important. This validates our assumption of negligible effects due to surface tension.

The case of the totally obstructing cylinder $a/d = 1$ deserves closer inspection. In this case, the trapped mode becomes an edge mode. It corresponds to the degeneracy of the symmetric and antisymmetric trapped modes and thus to the intersection between the two branches of resonance in fig. 7. Experimentally, the resonance frequency of the edge mode is found at $kd = 1.44$. The corresponding pattern of the edge mode is shown in fig. 8.

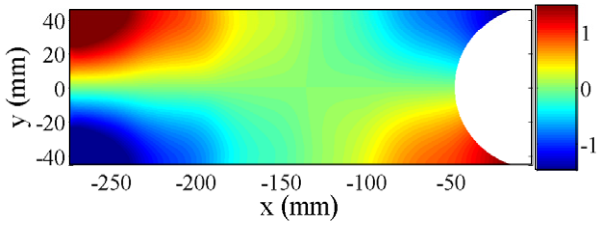

Fig. 8: (Color online) Edge mode experimentally observed for $a/d = 1$ and $kd = 1.44$. The scale of the colorbar is in mm.

* * *

This work is supported by the ANR project ANR-08-BLAN-01108 Tourbillonde.

REFERENCES

[1] Linton C. M. and McIver P., *Wave Motion*, **45** (2007) 16.
[2] Kaplunov J. D. and Sorokin S. V., *J. Acoust. Soc. Am.*, **97** (1995) 3898.
[3] Pagneux V., *J. Acoust. Soc. Am.*, **120** (2006) 649.
[4] Jones D. S., *Proc. Cambridge Philos. Soc.*, **49** (1953) 668.
[5] Ursell F., *J. Fluid Mech.*, **183** (1987) 421.
[6] Mc Iver P., *Q. J. Mech. Appl. Math.*, **44** (1991) 193.
[7] Evans D. V. and Linton C. M., *J. Fluid Mech.*, **225** (1991) 153.
[8] Parsons N. F. and Martin P. A., *J. Fluid Mech.*, **284** (1994) 359.
[9] Kurennoy S. S., *Phys. Rev. E*, **51** (1995) 2498.
[10] Fedotov V. A., Rose M., Prosvirnin S. L., Papasimakis N. and Zheludev N. I., *Phys. Rev. Lett.*, **99** (2007) 147401.
[11] Evans D. V. and Porter R., *Appl. Ocean Res.*, **19** (1997) 83.
[12] Duclos G. and Clement A. H., *Ocean Eng.*, **31** (2004) 1655.

[13] Hu X., Shen Y., Liu X., Fu R. and Zi J., *Phys. Rev. E*, **69** (2004) 030201.
[14] Hu X. and Chan C. T., *Phys. Rev. Lett.*, **95** (2005) 154501.
[15] Farhat M., Enoch S., Guenneau S. and Movchan A. B., *Phys. Rev. Lett.*, **101** (2008) 134501.
[16] Retzler C. H., *Appl. Ocean Res.*, **23** (2001) 249.
[17] Takeda M. and Mutoh K., *Appl. Opt.*, **22** (1983) 3977.
[18] Maurel A., Cobelli P., Pagneux V. and Petitjeans P., *Appl. Opt.*, **48** (2009) 380.
[19] Cobelli P., Maurel A., Pagneux V. and Petitjeans P., *Exp. Fluids*, **46** (2009) 1037.
[20] Callan M., Linton C. M. and Evans D. V., *J. Fluid Mech.*, **229** (1991) 51.
[21] Evans D. V. and Porter R., *J. Eng. Math.*, **35** (1999) 149.
[22] Linton C. M. and McIver P., *Handbook of Mathematical Techniques for Wave/structure Interactions* (CRC Press) 2001.
[23] Granot E., *Phys. Rev. B*, **65** (2001) 233101.